Microfluidics investigation of the effect of bulk nanobubbles on surfactant-stabilised foams

L A Labarre, Arnaud Saint-Jalmes, D Vigolo

Microfluidics investigation of the effect of bulk nanobubbles on surfactant-stabilised foams

L. A. Labarre[1], A. Saint-Jalmes[2], D. Vigolo[1,3,4,]*

(1) School of Chemical Engineering, University of Birmingham, Birmingham, B15 2TT, UK.

(2) Univ Rennes, CNRS, IPR (Institut de Physique de Rennes) - UMR 6251, F-35000 Rennes, France

(3) The University of Sydney, School of Biomedical Engineering, Sydney, NSW 2006, Australia

(4) The University of Sydney Nano Institute, University of Sydney, Sydney, NSW 2006, Australia

* daniele.vigolo@sydney.edu.au

KEYWORDS foam, nanobubbles, stability, microfluidics.

ABSTRACT

Hypothesis

In aqueous foams, the bubble size usually spans from tens of microns to centimetres. It is however possible to create much smaller and stable bubbles in solutions: the recently discovered nanobubbles have diameters well smaller than a micron. Many issues are still pending on nanobubbles, especially regarding their stability. Here, we address if and how the addition of nanobubbles may change the interfacial and foaming properties of surfactant solutions.

Experiment

Using a first microfluidic device, nanobubbles are added to surfactant solutions (SDS and Triton X-100 at different concentrations). A second microfluidic device then generates foams from these solutions. In parallel, we also report systematic results on the interfacial and bulk properties of such solutions.

Key findings

Finally, we show that nanobubbles have some effects on almost all the measured quantities; however, the most striking one is to enhance the foaming of the solutions having an initial poor foamability. These measurements provide us with a wide set of new results allowing us to draw a first multi-scale picture of how far nanobubbles could potentially act as foam boosters and stabilizers or could be implemented in colloidal formulation. Yet, more investigations are required to unravel the mechanisms leading to our results.

1/ INTRODUCTION

Stability is a key issue for many industrial processes involving aqueous foams. Foam evolution is primarily determined by three destabilising events namely, drainage, coarsening, and coalescence [1,2]. To prevent those events to occur, surfactants [3], nanoparticles [4,5], polymers [6], or a combination of the above [7] can be employed.

Despite the development and improvement of such combination, this is not always enough to ensure the optimal foam stability necessary for each specific application. For example, in enhanced oil recovery [8–10], foams are exposed to high-temperature and high-pressure conditions that make foam stability challenging.

One of the main goals of current foam formulation engineering is to reduce the environmental impact by decreasing the quantity of surface-active agents or replacing them by biocompatible and/or biodegradable surface active-agents. As an example, scientists have exploited bio-based and biocompatible products such as chitosan [11,12] to generate and stabilise foams. Nevertheless, the extraction and processing of these products remain costly. In this work, the feasibility to employ very small and stable objects, called nanobubbles, was studied.

In the last two decades, such nanobubbles were discovered and investigated [13,14]. There are two kinds of nanobubbles: surface nanobubbles defined as gas-filled spherical caps of 10 to 100 nm height and a contact line radius between 50 to 500 nm present on hydrophobic surfaces, and bulk nanobubbles described as gas-filled spherical bubbles with a diameter below 1 micron located in the bulk of an aqueous solution [15]. In this study, the focus is given to bulk nanobubbles.

These bubbles have been introduced and employed in a wide range of applications from surface cleaning [16,17] to froth flotation [18,19] because of their extraordinary stability. This super stability is not fully understood but the main theories considered the bubble surface charge density [20] as the determining factor for their stability. Indeed, the ion-stabilisation model [21] explains

the single nanobubble stability by the existence of an electrostatic pressure that balances the high internal Laplace pressure. Additionally, the DLVO theory describes successfully the dependence of bulk nanobubbles cluster stability on parameters such as pH and electrolytes in solution [20].

Two studies conducted by Ushida *et al.* (2012) and later Yesui *et al.* (2018) showed that the presence of nanobubbles in solution could affect various gas-liquid interfacial properties [22] [23].

The important role of nanobubbles on the stability of nanoparticles dispersions was also recently demonstrated. Zhang and Seddon (2016) highlighted a potential nucleation or attachment of nanobubbles onto negatively charged gold nanoparticles above a threshold nanoparticle size [24]. Zhang et al. (2019) found that the ratio of nanoparticle to nanobubbles in solution could be used to tune the zeta potential of the resulting dispersion of initially positively charged Polystyrene latex nanoparticles [25].

Another recent work was dedicated to the study of the combination of nanobubbles with various frothers and/or hydrophobic nanoparticles and their impact on the separation efficiency in the froth flotation process [19,26–29]. Sobhy and Tao (2019) found for the first time, that froth stability was improved by nanobubbles in the presence of strongly hydrophobic particles [27].

Thus far, few studies have been undertaken to determine if these nanobubbles could affect dispersed colloidal systems such as foams or emulsions.

Therefore, this work investigates for the first time how nanobubbles generated by microfluidics in a well-controlled and reproducible way could affect aqueous surfactant stabilized foams (also produced by microfluidics). In each foam study case, the nanobubble-surfactant solution properties, their foamability and the resulting foam properties are analysed and compared to the properties of the foam stabilised by surfactant only.

First, the materials and methods employed in this work are described. The results – obtained for two different surfactants and at various concentrations – are then discussed at each relevant length

scale for foams: from the microscopic scale of the gas-liquid interface, to the bubble-scale in bulk, and up to the foam itself.

2/ MATERIAL & METHODS

2.a Materials

Two surfactants were studied: Sodium Dodecylsulfate (SDS), an anionic surfactant, and, 2-[4-(2,4,4-trimethylpentan-2-yl)phenoxy]ethanol named Triton X-100 (TX100), a non-ionic surfactant. SDS (AR > 99%) and TX100, laboratory grade were purchased from Sigma-Aldrich. All the foaming solutions were prepared by mixing with a magnetic stirrer at 25°C the surfactant in Millipore water (18.2 mS m^{-1} conductivity) to achieve complete dissolution. A 0.2 µm Acrodisc syringe filter was used to filter all the stock solutions. These two types of surfactant were investigated at four concentrations: 0.5, 1, 2.5 and 5 times their critical micellar concentration (cmc). The cmcs were found in the literature at 6.0 x 10^{-4} mol L^{-1} - for TX100 and 8.3 x 10^{-3} mol L^{-1} for SDS at 25°C [30–32]. It should be noted that TX100 presents a cmc more than 10 times smaller than SDS.

2.b Bulk nanobubble generation via microfluidics

The silicon mould used to make the two-depth microfluidic device was purchased externally from the Nanofabrication Centre (Southampton, UK). Microfluidic devices were fabricated in Polydimethylsiloxane (PDMS, Sylgard™ 184 Silicone Elastomer Kit, Dow Chemical) by soft lithography [33,34]. The PDMS devices were then irreversibly bonded to a microscope glass slide by corona discharge [35]. In order to assure a homogeneous foam formation in the channel [36], the devices were surface treated to become hydrophilic with a layer-by-layer technique by flowing alternated segments of prop-2-en-1-amine;hydrochloride (PAH, Sigma Aldrich) and 4-ethenylbenzenesulfonic acid (PSS, Sigma Aldrich) solutions (both 0.1% w/v in 0.5 M aqueous sodium chloride, NaCl solution) with aqueous NaCl washing solution (0.1 M) segments in between

as described in [37]. The two-layer microfluidic device used for nanobubble generation was similar to the one described in Evans *et al.* [38,39]. It was made by PDMS and consisted of two regions with different depths (d_1 = 25 μm and d_2 = 55 μm): the shallow zone contained a flow-focusing junction where the 50 μm wide gas inlet met with two 100 μm wide liquid inlets. The channel then suddenly expanded in both width (up to 280 μm) and depth as depicted in Figure 1. One reservoir of air was connected via a pressure controller (OB1 MK3, Elveflow) to the gas inlet via 0.020" x 0.060" OD Tygon microbore tubing (Cole-Parmer Instrument Co. Ltd., UK) to accurately control the gas inlet pressure. A 10 mL syringe filled with the sample was connected to the liquid inlet via the same tubing, and its flow rate was finely controlled with a syringe pump (Harvard Syringe Pump 11 Pico Plus Elite, Harvard apparatus). The liquid flow rate was set at 90 μL min^{-1} and the gas inlet pressure was fixed at 1000 mbar. The microfluidic device used for the generation of nanobubbles was cleaned thoroughly by flowing pure water at 90 μL min^{-1} for 10 min prior to any experiment. A 1 mL nanobubble sample was collected into a disposable plastic cuvette and/or into a clean and dry glass beaker at the channel exit.

One of the main peculiarities of this design is the change in depth between the nozzle and the expansion channel. To produce an atomization-like spray, the depth was more than doubled (from d_1 = 25 μm to d_2 = 55 μm) so that the pressure drop was abruptly changed [38,39]. The drop in pressure led to hydrodynamic cavitation and to the bulk nanobubbles generation.

The nanobubbles concentration after one generation cycle was assumed to be about 10^9 bubble mL^{-1} based on the similar experimental conditions (device geometry, flow rate and pressure) employed by Evans et al. [38,39].

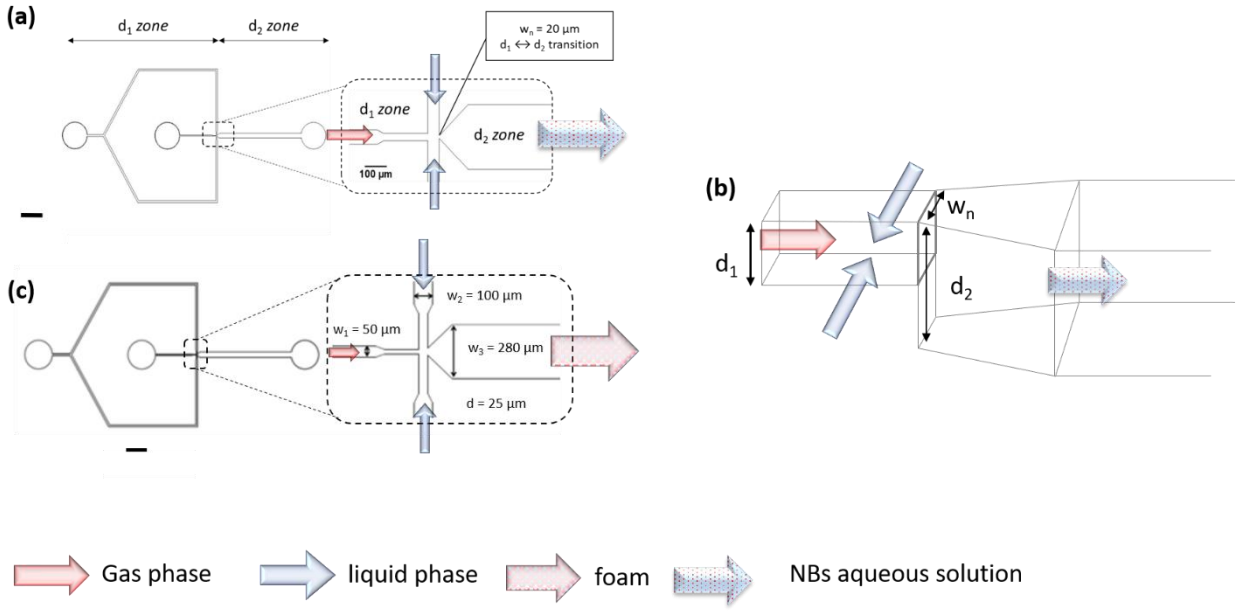

Figure 1 (a) schematic of the two-depth (d_1 = 25 µm & d_2 = 55 µm) flow-focusing device (left) and a zoomed in view of the two-depth flow focusing junction (right) for bulk nanobubbles generation. (b) Schematic representation of the cross-sectional view of flow-focusing two-depth device employed for bulk nanobubbles generation. (c) Schematic of the 25 µm depth flow-focusing device (left) and a zoomed in view of the flow focusing junction (right) for foam generation. Scale bar = 1000 µm.

2.c Interfacial & bulk characterisation

The presence of nanobubbles and their size distribution in pure water and in surfactant solutions were analysed at 25 °C by dynamic light scattering (DLS, Zetasizer NanoZSP, Malvern Instruments Ldt) before and after the microfluidic foaming of the resulting solutions.

The zeta potential of the various nanobubble solutions was measured using a Zetasizer NanoZSP (Malvern instruments Ltd). This measurement was done before and after the foaming of the solutions; in the latter case, the foam was left to drain and the resulting liquid was collected and analysed for each condition.

The temporal evolution of the surface tension at short timescales (down to 1 ms) of the surfactant solutions were also analysed with a maximum bubble pressure tensiometer (Sinterface BPA-1). This method allows for the measurement of the maximum pressure that needs to be applied to

create and detach a bubble at the tip of a 0.13 mm diameter capillary placed vertically in a liquid [40].

2.d Foam generation & analysis

A foam was generated by co-injection of a foaming solution and air in a 25 µm depth flow-focusing device described in Figure 1 (c). The gas and liquid inlet pressures were controlled by a pressure controller and set at 1000 mbar and 1900 mbar respectively. The foam was formed and studied downstream in the 280 µm wide channel. The foam was then collected into a glass cuvette (0.4 x 0.8 mm), previously cleaned with water and ethanol and dried with air, via a 15 cm length tubing, 0.020" x 0.060" OD Tygon microbore tubing (Cole-Parmer Instrument Co. Ltd., UK). The foaming time was fixed at 1 minute after the first bubble exit the tubing and entered the glass cuvette.

In this work, the foamability was evaluated by the initial foam heights (Figure 6), initial liquid fractions (Figure 7) and qualitatively by microscopy observations (Figure 8). For the latter, a small amount of foam, taken at the early stage of its life, was deposited on a glass slide, and covered with a cover slip.

The height evolution of the foam was measured manually by following the foam column height (difference between the top and the bottom of the foam column) over time. The foam height was normalised by the value obtained after 1 min (end of the foaming process) to study its evolution.

The liquid fraction was evaluated by weighting the amount of liquid left in the cuvette (m_L) once the foam had drained. The initial uniform foam liquid fraction (φ_L) was computed from the following expression:

$$\varphi_L = \frac{V_L}{V_{foam}} = \frac{m_L}{h_{foam}\ A_{cuv}\ \rho_L} \qquad [1]$$

where, h_{foam} is the initial foam height, A_{cuv}, the cross-section of the measuring cylinder and ρ_L, the volumetric mass density of the foaming liquid.

3/ RESULTS ON INTERFACIAL PROPERTIES OF SURFACTANT SOLUTIONS

The short timescale tensiometry results are presented in Figure 2.

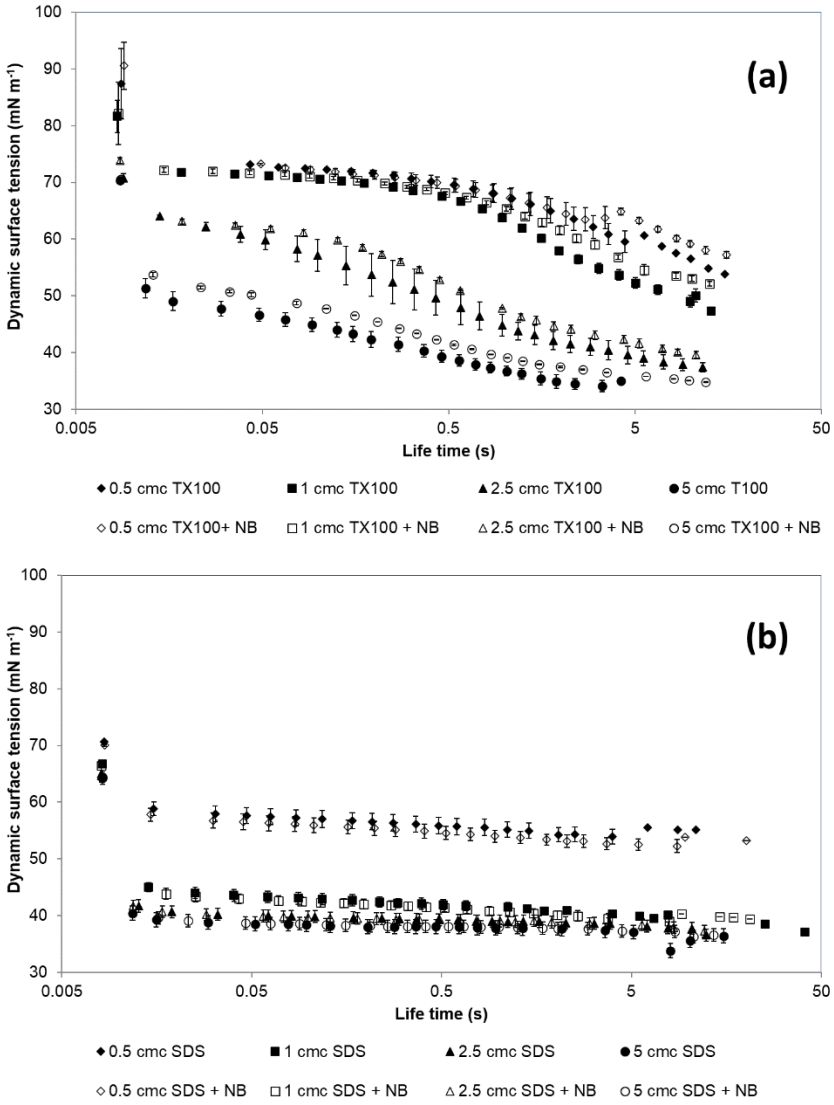

Figure 2 Dynamic Surface Tension results for the set of TX100 (a) and SDS (b) solutions from 0.5 (♦,◊), 1 (■,□), 2.5 (▲,Δ and 5 cmc (●,○) described by filled symbols for surfactant solutions and by unfilled symbols for nanobubble-surfactant solutions. The error bars are standard errors.

Overall, the results for the pure surfactant solutions were consistent with the literature. The difference between TX100 and SDS solutions resided in the dynamics of adsorption. Indeed, the most important contribution is the characteristic adsorption time that depends on the diffusion coefficient of the surfactant, but also quadratically on the concentration [41]. As TX100 and SDS have different cmcs, their absolute concentrations are different if one uses them at constant cmc units as in our case. Consequently, SDS molecules diffuse at an interface and cover it faster than TX100 molecules. Even above the cmc, the equilibrium is only reached in a few seconds for TX100 solutions, while equilibrium is quasi-instantaneous for SDS solutions at all concentrations.

The choice of surfactant and concentration allowed for the full range coverage of possible interfacial dynamics: at a typical timescale of 1s – time required for producing a bubble in the foaming device – experiments could be performed with almost bare interfaces (for the lowest TX100 concentrations) up to fully saturated interfaces (for the highest concentrations of SDS).

The nanobubble action on the interfacial properties varied with the surfactant type and concentration for a fixed nanobubble concentration.

Qualitatively, a possible impact of nanobubbles (NBs) on the interfacial properties was only observed for solutions of TX100, but this impact appears small. Oppositely, for SDS solutions, the presence of nanobubbles did not impact the dynamic surface tension.

To quantitatively evaluate the differences between the NBs and non-NBs solutions, an ANOVA statistical analysis was performed to evaluate the impact of nanobubbles on the surface tension measurement over the whole spectrum of bubble life time per surfactant concentration and surfactant type presented in Figure 2. The results are summarised in **Table S1** in the Supplementary Material section.

Despite, the results of the ANOVA test showing that there was no significant difference (p-value > 0.05) caused by the presence of nanobubbles for the whole range of surfactant concentration, the

p-values for TX100 are clearly smaller than for SDS except at 0.5 cmc, showing that the NB could have a greater impact on TX100 than on SDS interfacial properties.

Indeed, from Figure 2 (a), from 0.5 to 5 cmc, the nanobubble-TX100 solution surface tension was always greater than the reference towards the longest timescales (after 5s at 0.5 cmc, and throughout the whole dynamical range at 5 cmc).

4/ RESULTS ON BULK PROPERTIES OF SURFACTANT SOLUTIONS

4.a Gaseous nature of bulk nanobubbles in pure water

The nature of the nano-entities generated from pure water by the 20 µm nozzle two-depth microfluidic device was verified to be nanobubbles. Following what was discussed by Nilmalkar *et al.* (2018), the gaseous nature of bulk nanobubbles was simply demonstrated by freezing a vial containing an aqueous solution of bulk nanobubbles generated by microfluidics, by dipping it for 30s in liquid nitrogen and by thawing it at room temperature for a whole day [42]. After this step, no nanobubbles were detected via DLS. This result demonstrated that nanobubbles were made of gas as solid impurities would have otherwise remained in solution and eventually agglomerated after thawing. The histograms in Figure 3 represent the size distribution evolution obtained 30 minutes, 1 week and 1 month after microfluidic generation.

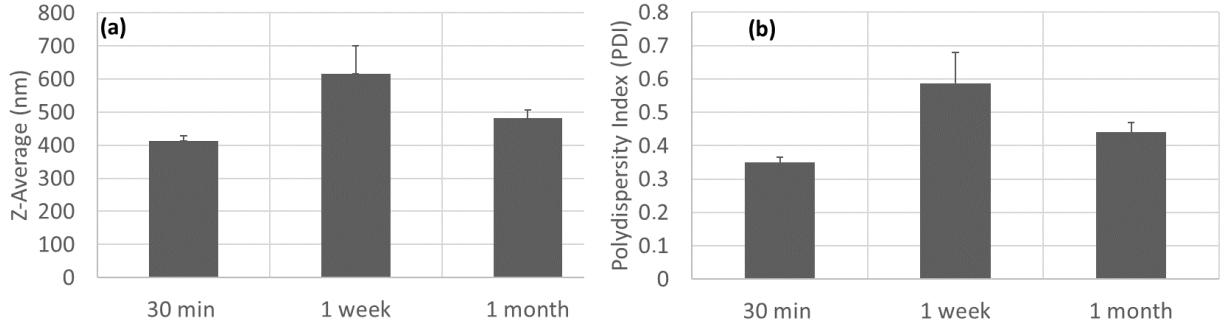

Figure 3 Z-average diameter (a) and polydispersity (b) evolutions for the nanobubble dispersion in pure water generated by the 20 µm nozzle microfluidic device. The error bars are standard errors.

The evolution of the Z-average and polydispersity index (PDI) suggests that after one month, the nanobubbles were still stable in solution.

4.b Nanobubble-surfactant dispersions

The nanobubble size distributions in the presence of surfactant are given in Figure 4 for the different concentrations investigated (denoted "NB"). For comparison, equivalent distributions after the microfluidic foaming process (denoted "NB foamed") were obtained from the analysis of the foam drained liquid and are also reported in Figure 4.

It was observed that the foaming process did not affect significantly the nanobubble-surfactant distributions as the sizes were similar throughout the different concentrations before and after foaming. An exception was visible at a SDS concentration of 0.5 cmc: the foaming process caused a strong increase in the nanobubble average size. This trend was confirmed by the ANOVA statistical analysis p-value obtained at 0.5 cmc for the PDI evolution before and after foaming. The results can be found in the **Table S2** in the Supplementary Material section.

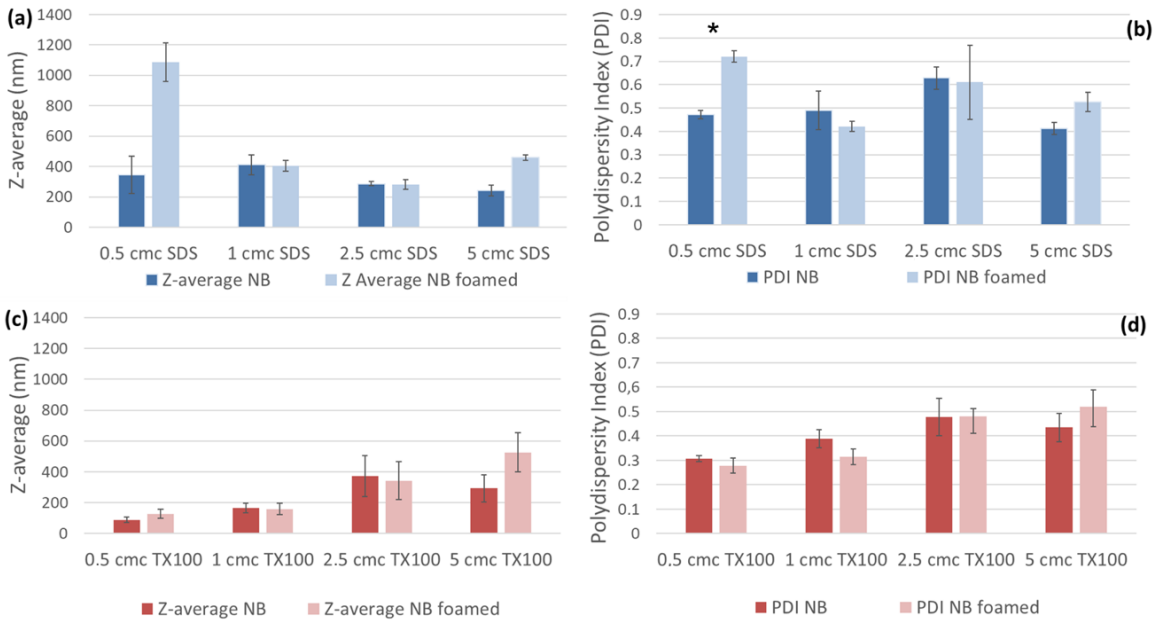

Figure 4 Z-average diameter (a,c) & Polydispersity (b,d) evolutions for the nanobubble-surfactant dispersions before and after foaming for the four SDS and Triton X-100 surfactant concentrations. The error bars are standard errors. Based on the ANOVA test, the asterix " * " describes a p-value below 0.05.

4.c Zeta potential

The evolution of the zeta potentials of the surfactant solutions containing NB was studied before and after the foaming process, and for each concentration, as depicted in Figure 5.

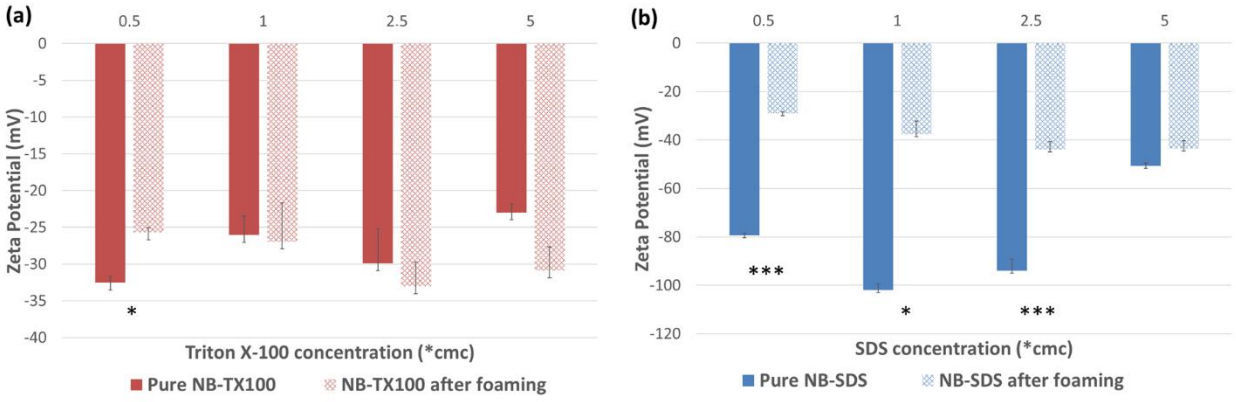

Figure 5 Zeta potential evolution of the nanobubble-surfactant dispersion in water for various Triton X-100 (a) and SDS (b) concentrations (0.5, 1, 2.5 and 5 cmc) before (dark red and blue) and after foaming (light red and blue). The error bars are standard errors. Based on the ANOVA test, the asterix " * " describes a p-value below 0.05, " ** " means a p-value below 0.005 and " * " p-value below 0.0005 respectively.**

An ANOVA statistical analysis was performed to determine in which case the *foaming process* had a significant effect or not on the nanobubble population.

The results of the ANOVA statistical analysis are summarised in **Table S3** in the Supplementary Material section.

From Table S3, it appeared that the foaming process significantly impacted the zeta potential only at 0.5 cmc TX100. A second ANOVA statistical analysis was performed to evaluate the effect of *TX100 concentration on the zeta potential either before, or after foaming*. First, for TX100, from Figure 5 (a), it was found that by increasing the surfactant concentration in solution, the zeta potential before foaming appeared almost constant, possibly just being slightly decreased. The steadiness of the zeta potential before and after foaming was confirmed with a p-value of 0.69 and 0.21 obtained for the four groups of concentration respectively demonstrating that the various concentrations analysed showed similar zeta potentials.

For SDS, in Figure 5 (b), it was found that from 0.5 to 2.5 cmc, the initial nanobubble-surfactant dispersions exhibited a large negative zeta potential varying from -80 to -100 mV. Only the 5 cmc SDS sample showed a smaller zeta potential of -40 mV. Very negative values were also reported in the literature for the combination of SDS and nanobubbles generated via ultrasonic cavitation [20]. Based on this paper, SDS was said to enhance the nanobubble charge density in solution.

After foaming, the zeta potential for the three lowest concentrations dropped by half, ranging from -25 to - 40 mV. A first ANOVA statistical analysis was performed to evaluate the effect of the foaming process on the zeta potential. A second analysis was realised to study the effect of the SDS concentration on the zeta potential before and after foaming. The strong effect of the foaming process on the nanobubble-SDS dispersions zeta potential was confirmed by the p-values summarised in **Table S3** for each concentration.

Similarly, the significant effect of the SDS concentration on the zeta potential before and after foaming was confirmed with a p-values of 4.9×10^{-4} and 8.3×10^{-3} respectively obtained for the four concentrations demonstrating that the various groups analysed were significantly different.

All in all, for SDS, *both surfactant concentration and the foaming process* had a significant impact on the zeta potential. For TX100, the effect of the foaming process varied with the concentration whereas the concentration had no significant impact on the zeta potential either before or after foaming.

5/ RESULTS ON FOAMS

5.a Foamability

In this section, the foamability was evaluated by the initial foam heights (Figure 6), initial liquid fractions (Figure 7) and qualitatively by microscopy observations (Figure 8).

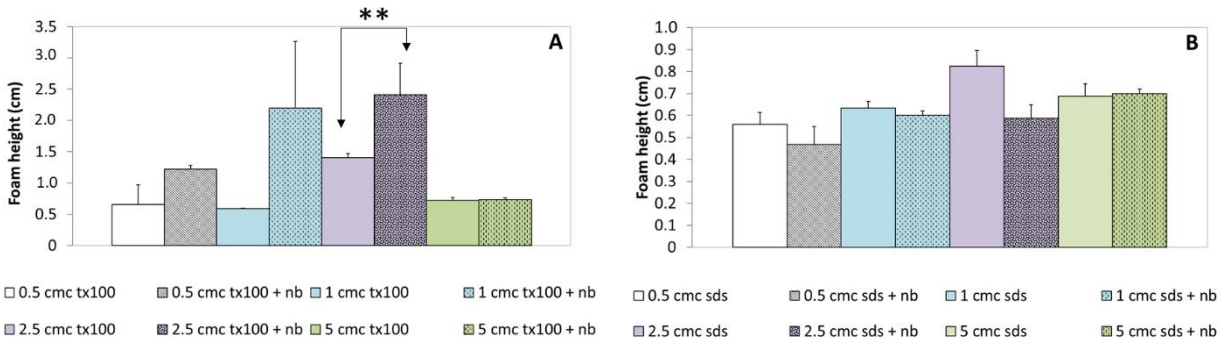

Figure 6 Foam height after 1-minute foaming for 0.5 (white), 1 (blue), 2.5 (purple) and 5 (green) cmc Triton X-100 (A) and SDS solutions (B) (blank) versus bulk nanobubbles + Triton X-100 and SDS solutions respectively (symbols). The error bars are standard errors. Based on the ANOVA test, the asterix " ** " means a p-value below 0.005.

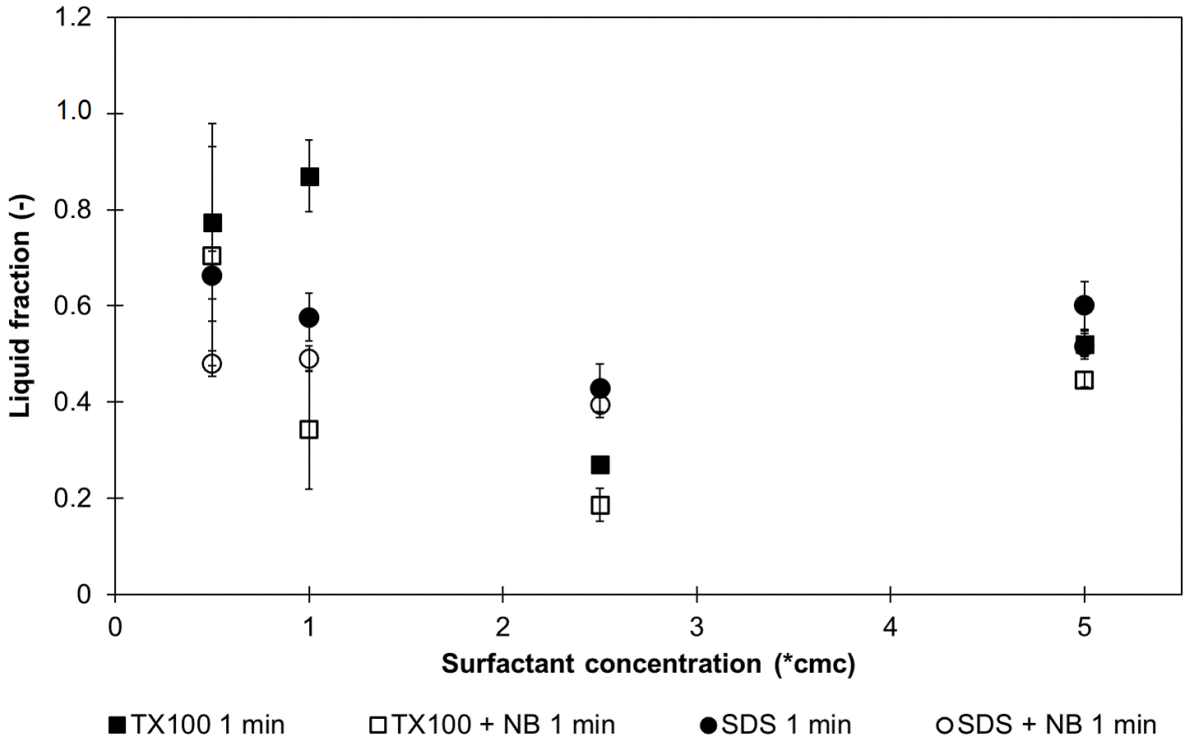

Figure 7 Foam liquid fraction evolution for Triton X-100 (square) and SDS solutions (circle) (filled symbols) versus bulk nanobubbles + Triton X-100 and bulk nanobubbles + SDS solutions (unfilled symbols). The error bars are standard errors.

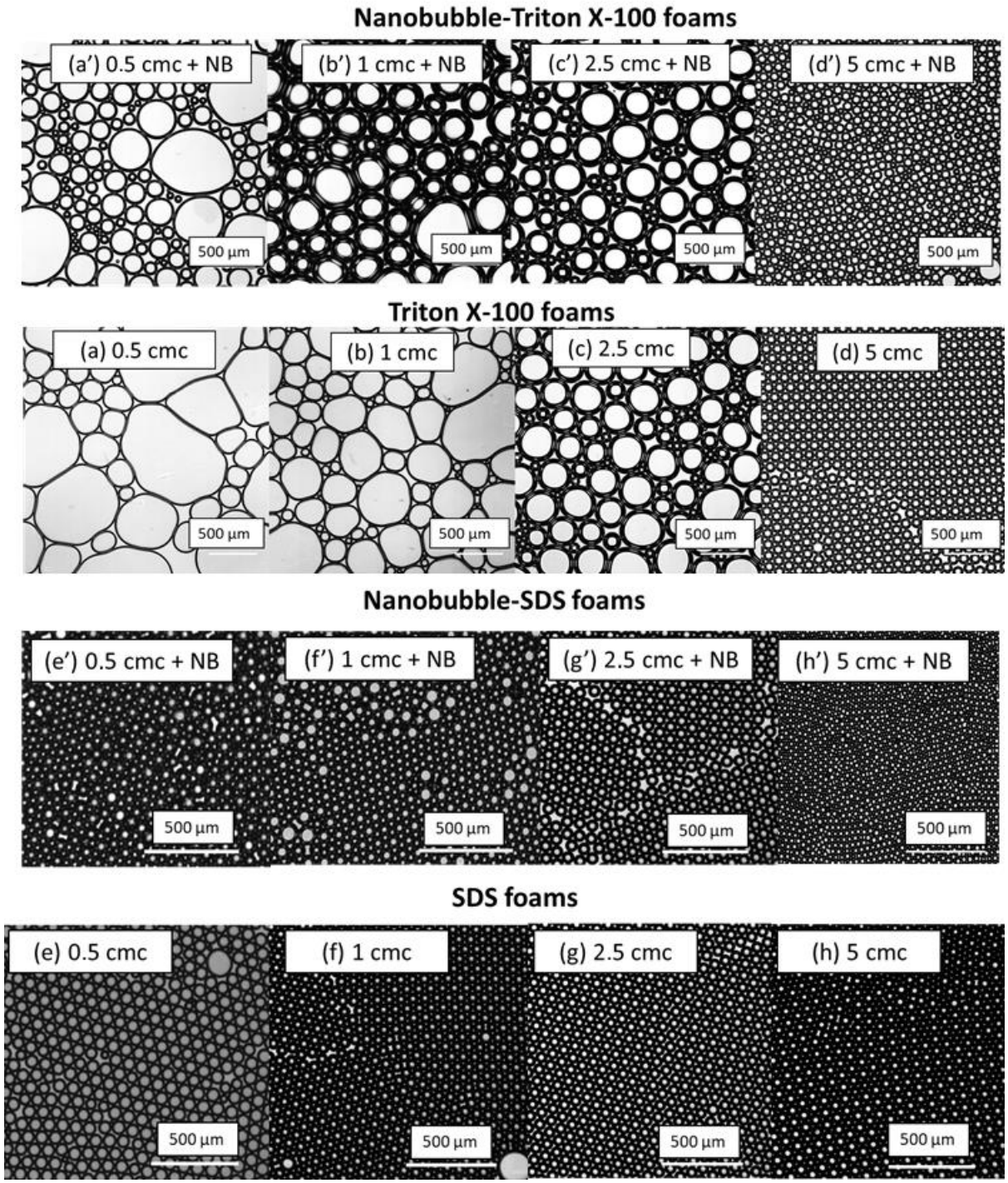

Figure 8 Foam after 5s deposition on a glass slide under a cover slip for various concentrations of Triton X-100 (0.5 (a), 1 (b), 2.5 (c), 5 (d)) cmc solutions & Triton X-100 – nanobubble solutions at 0.5 (a'), 1 (b'), 2.5 (c') and 5 cmc (d') and of SDS (0.5 (e), 1 (f), 2.5 (g), 5 (h)) cmc solutions & SDS – nanobubble solutions at 0.5 (e'), 1 (f'), 2.5 (g') and 5 cmc (h').

5.1.a. SDS: Optimum foaming conditions with & without NB

First, it was noted that the device created "wet" foams, as the liquid fractions were always about 0.5. Accordingly, all the foam pictures showed closed (but not packed) spherical bubbles.

From Figure 6, the initial foam height after 1 min was almost constant, independent from the concentration and from the presence of NB.

An ANOVA statistical analysis was performed to determine the *effect of the concentration* on the foam height and liquid fraction after 1 min in the case of the pure SDS solutions and SDS-NB solutions. An additional analysis was realised to evaluate the *effect of nanobubbles presence in SDS solutions* for the four concentrations investigated.

The results reported in **Table S4** in the Supplementary Material section showed that the concentration did not impact significantly the foam height and the liquid fraction after 1 min for the pure SDS and SDS-NB solutions. Furthermore, it was confirmed with the second ANOVA analysis that NB had no, or only a small impact on the foaming of SDS solutions, in the investigated range of concentration.

This set of foamability results showed that - for SDS solutions for all concentrations, which can be considered as solutions of **optimum foamability** - the device was producing about 0.6 – 0.7 cm of foam in 1 min. The initial microbubble sizes were almost all equal (45 ± 5 µm) as depicted in Figure 8.

Additionally, the impact of nanobubbles on the capture of free surfactants in solution and its resulting effect on the number of available surfactant molecules for foaming were evaluated. The following expression was used to assess the number of surfactant molecules N_S of area A_S employed to cover a bubble surface of radius R_B [23]:

$$N_s = \frac{4\pi R_B^2}{A_S} \quad [2]$$

The surface to cover comprised the total amount of nanobubbles in the liquid contained within the foam and an additional surface from the microbubbles once the solution containing the nanobubbles was foamed. The areas per surfactant molecule were approximated at 50 and 65 Å² respectively for SDS and TX100 based on the literature [43,44]. The number of nanobubbles for 1 m^3 was set at 10^{15} nanobubbles. The nanobubbles diameters employed for the calculation were taken from Figure 4. The microbubbles diameters were estimated from the image analysis of a series of snapshots like the one in Figure 8. In this calculation, an irreversible adsorption of surfactant on nanobubble/microbubble surface was considered to simplify the estimation. The detailed figures are available in **Table S7 and Table S8** in the supplementary material section.

The calculation showed that the required number of surfactants to cover NB (row E in Table S7 and S8) is always *orders of magnitude smaller* than what is required to cover the MB (row D in Table S7 and S8).

Despite the large number of NB, they represent a small surface to be covered compared to the surface of microbubbles. Consequently, in terms of surfactant adsorption, the nanobubbles captures negligible amount of surfactant when compared to the microbubbles.

Moreover, there was always enough SDS molecules to cover all the MB, even at the lowest surfactant concentration (Table S7, row G > row F). This calculation was consistent with the experimental data: *all SDS-NB solutions showed optimum foaming even at the lowest concentrations, and NB did not impact the foaming efficiency by immobilizing free surfactants*. Therefore, from Figure 6, Figure 7 and Figure 8, it was concluded that SDS solutions could be

considered here as “references” in terms of optimum foaming properties for all the concentrations and conditions (with or without NB), under the microfluidic foaming process used here.

5.1.b. TX100 foams: smooth transition from poor to good foaming (P/G foaming)

At 0.5 cmc TX100, a very poor foamability was obtained: the liquid fraction was high (> 0.7) corresponding to low gas incorporation, and to a 'bubbly liquid' rather than a foam. Moreover, the bubbles coalesced very fast, as the liquid drained out rapidly. As a consequence, it was impossible to perform relevant microscopic observation of the produced bubbly liquid; instead, as shown in Figure 8 (a) only a small number of large coalesced bubbles remained after deposition. At 1 cmc TX100, similar unstable foam behaviour was observed despite slightly more foam produced. The foaming properties improved significantly at 2.5 cmc: the foam height doubled with respect to 1 cmc, and the liquid fraction decreased significantly from 0.8 to 0.3 meaning packed bubbles within a foam, and no longer a bubbly liquid.

Finally, at 5 cmc, the foam showed optimum foaming properties and recovered an SDS-like behaviour. This last set of results at 5 cmc validated the control over our setup and analysis: each system (SDS or TX100) showed similar properties (liquid fraction, height, structure) once the concentrations were well above the cmc.

Thus, from 0.5 to 5 cmc, pure TX100 solutions exhibited a smooth transition from poor to good foaming. Figure 8 (a-d) showed – oppositely to SDS (Figure 8 e-h) – how the foam quality increased with the concentration: it was only at the highest concentration that the optimal foamability (being defined as the one of SDS) was recovered.

At intermediate concentration (2.5 cmc), the foam height was the highest: this result might have looked inconsistent with the previous observation that the foamability of TX100 is optimal and equal to the one of SDS, only at 5 cmc. However, such foam height comparisons must only be

made *at the same bubble sizes*. In fact, the foam viscosity increases strongly as the bubble size decreases. In the setup, *the pressure was controlled, not the flow rate*. Therefore, as bubbles got smaller, a higher pressure would be required to push the foam at similar flow rates. Here, the pressure was kept constant, therefore the flow rate – and thus the total height of the foam made - had decreased.

At 0.5 cmc of TX100 *with added NB*, the foamability stayed poor as shown in Figure 8 (a') with the presence of large bubbles due to coalescence, and with the same value of high liquid content of 0.75.

Yet, the foamability of the TX100-NB compared to TX100 solution was enhanced: the foam height for TX100-NB was almost doubled compared to the TX100 foam as shown in Figure 6.

At 1 cmc TX100-NB, the presence of nanobubbles increased the foam height compared to the TX100 foam despite a slight reduction of bubble size. Figure 8 (b') showed that, thanks to the presence of NB, the structure of a foam is obtained. Consequently, the liquid fraction was much lower for the TX100-NB foam and the NB-doped solution was able to incorporate gas more efficiently. At 2.5 cmc, the TX100-NB solution presented a higher foamability (foam height of 2.4 cm) than TX100 (foam height of 1.4 cm) for a similar range of bubble sizes (Figure 8 (c) for TX100 & (c') for TX100-NB).

At 5 cmc TX100, both foams reached the same height, foam structure and liquid fraction describing optimum foaming conditions. The liquid content in both cases had reached 0.5 at 5 cmc for TX100 foam and 0.41 at 5 cmc for TX100-NB foam. The strong decrease in foam height from 2.5 to 5 cmc for both foams was again explained by the increase in foam viscosity linked to the decrease of the microbubble diameters.

It thus turned out that, in the presence of NB, a similar transition - from poor to optimal foaming - was observed but *was shifted towards lower concentrations of TX-100*.

Therefore, nanobubbles helped foaming in the range of concentration where the foaming was poor (0.5, 1 and 2.5 cmc TX100). This was visible in Figure 8 (a' – c') (smaller bubbles), in the liquid fractions (Figure 7), and in the foam height (Figure 6) which was much greater with NB especially in conditions providing the same bubble size (e.g., 2.5 cmc). Thus, NBs played a "foam booster" role in the P/G transition range.

The nanobubbles effect per concentration on the foam height and liquid fraction was evaluated by ANOVA statistical analysis. The p-values obtained are gathered in **Table S5** in the Supplementary Materials section. This analysis confirmed the trend observed qualitatively and notably that the effect of nanobubbles on the foam height distribution of TX100 foams was the strongest at 2.5 cmc. An additional ANOVA statistical analysis was also employed to evaluate the effect of the TX100 concentration on the foam height and liquid fraction after 1 min foaming. As summarised in the supplementary material section below Table S5, it was found that the surfactant concentration did not significantly impact the liquid fraction after 1 min for the pure TX100 and TX100-NB solutions.

Nevertheless, the analysis highlighted the fact that the concentration originally impacted significantly the evolution of the foam height for the pure TX100 solution ($p<0.005$) but the addition of nanobubbles caused the concentration to have a lesser impact on the foaming properties. This change is an indicator of the foam "boosting" effect of nanobubbles on the whole range of TX100 concentrations as the foaming properties become less dependent upon the surfactant concentration thanks to the presence of nanobubbles in solution. Indeed, as seen for SDS (optimum foaming properties), both concentrations and nanobubbles have no impact on the foam height and on the liquid fraction.

In addition, Equation 2 was employed at 0.5 cmc TX100 to determine the number of TX100 surfactant molecules required to cover NBs and MBs.

At 0.5 cmc, SDS solutions presented 35 times more molecules than TX100 due to the different values of cmc for the two surfactants. As a consequence, at the lowest concentration, the amount of free TX100 molecules is comparable or lower to the one required for covering all the MB (**Table S8** in the supplementary material section). Despite the rough approximation in this calculation, this explained the poor foaming of TX100 at low concentrations (together with adsorption dynamics shown in Figure 2). Note also, that – as for SDS - the required number of surfactant molecules to cover the NB (row D in Table S7 and S8) is always orders of magnitude smaller than what is required to cover the MB (row E in Table S7 and S8). Consequently, the presence of nanobubbles can be neglected for both surfactants.

5.b Foam stability: time evolution

The foam stability was quantified by comparing the normalised foam height evolution reached after 10 min as described in Figure 9.

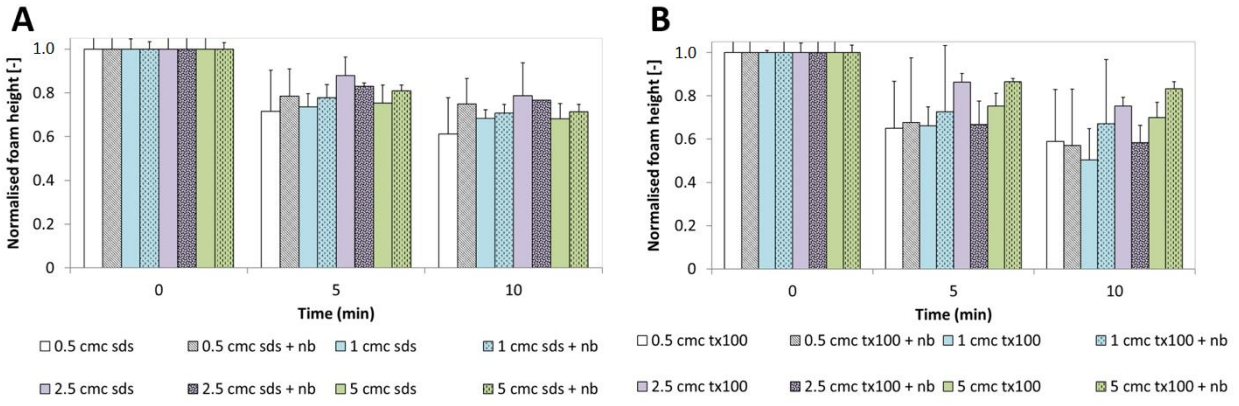

Figure 9 Normalised foam height evolution at 5 and 10 minutes after foaming for 0.5 (white), 1 (blue), 2.5 (purple) and 5 (green) cmc SDS (A) and TX100 solutions (B) (solid colour) versus bulk nanobubbles + Triton X-100 and SDS solutions respectively (coloured lattice). The error bars are standard error bars.

Foams made of TX100 were generally more unstable than the SDS foams: in average, the height was halved in 15 minutes, while it was still 2/3 of the initial foam height for SDS after 20 minutes. This showed that drainage and coalescence occurred within these foams.

An ANOVA statistical analysis was firstly used to determine the impact of the presence of nanobubbles on the normalised foam height after 10 minutes for each surfactant concentration. Secondly, the same method was employed to determine the impact of surfactant concentration on the foam stability, symbolised by the evolution of the normalised foam height after 10 minutes.

For SDS, the surfactant concentration did not impact significantly the foam height evolution after 10 minutes, as determined by the p-values of 1.0×10^{-1} and 1.7×10^{-1} obtained respectively for the SDS and SDS-NBs sets. The effect of the presence of NBs was assessed for each concentration. The p-values are gathered in **Table S6** in the Supplementary Materials section.

Based on those p-values, it can be concluded that the presence of nanobubbles in SDS solutions didn't affect significantly the foam evolution 10 minutes after its generation by microfluidics. The surfactant concentration impacted significantly the foam height evolution after 10 minutes for TX100 foams ($p = 5.0 \times 10^{-3}$). Oppositely, it did not affect significantly the foam height after 10 minutes for the TX100-NBs set. Thus, for TX100 foams, the stability after 10 minutes was higher at 2.5 and 5 cmc. The effect of the presence of NBs was assessed for each concentration. The p-values are gathered in **Table S6**. Those results demonstrated that the presence of nanobubbles in TX100 solutions did not influence significantly the foam evolution 10 minutes after its generation by microfluidics.

To summarise, further investigation with larger foam volumes, other ranges of liquid fractions and bubble sizes, will be required to better determine the real impact of the nanobubbles on the foam aging mechanisms.

6/ Summary & Perspectives

With our microfluidic setup, when foamability was optimum, wet foams of small bubbles were obtained with liquid fraction of 0.5 for both surfactants.

Taking together all the dimensions at stake, nanobubbles showed limited effect on SDS solutions: for the exact same foaming process, similar interfacial properties resulted in the generation of high-quality foams for the whole range of concentrations.

However, the action of nanobubbles remained unclear regarding the change of zeta potential and size of nanobubbles induced by the foaming process at the lowest SDS concentration. Further work needs to be done, in particular at concentrations much lower than what was tested here, where it could be possible to investigate the poor to good foaming transition and the role of NBs on it. Nanobubbles may then have an impact on SDS concentrations for which the foaming was low, typically comparable to the one at 1 cmc of TX100.

At low TX100 concentrations, poor foamability was obtained, correlated to the high values of dynamic surface tension and the low number of free surfactants for foaming. Unlike SDS, the increase in surfactant concentrations improved the foaming process for TX100 with a shift from a very unstable foam to a stable one at 2.5 cmc. The presence of nanobubbles in solution significantly impacted the foam quality at low and intermediate concentrations: the transition from poor to good foaming was shifted towards lower concentrations.

At fixed bubble size, the effect of nanobubbles improved the foamability at 2.5 cmc TX100. Indeed, a higher foamability in the presence of NBs at low and intermediate concentrations of Triton X-100 was obtained.

Regarding the mechanism by which NBs are acting on foaming, various scenarios can be proposed: on one hand, nanobubbles could act as particles and stabilize the foam by adsorbing at the interface. On the other hand, NBs could help releasing large amount of surfactant when adsorbing at gas-liquid interface, thus acting as surfactant reservoirs by “freeing” surfactant initially present at the interface. Furthermore, NBs could have a “bulk” effect and prevent two microbubbles from getting too close and coalescing. The adsorption of negatively charged nanobubbles at the foam gas-liquid

interface could increase the electrostatic repulsion between the two interfaces and prevent them from getting in contact and break. The surfactant adsorption on the nanobubble surface could also help the nanobubble adsorption at the gas-liquid interface (microbubble). More experiments at the scale of single thin films will then be required to unravel the mechanism by which NBs play a role in foam stability.

7/CONCLUSION

Summary of key findings

This work introduced an original multiscale, controlled, and systematic study of the effect of bulk nanobubbles on aqueous foams generated by microfluidics for two different surfactants over a broad range of concentrations.

Herein, for the first time, the effect of the presence of nanobubbles on interfacial properties, on the bulk and on foam properties (foamability and foam stability) was systematically studied. Several discoveries were made:

(i) Nanobubbles can have an impact on foams made of microbubbles;

(ii) The impact of the presence of nanobubbles is more evident at low and intermediate surfactant concentrations where NBs enhanced the foamability;

(iii) Nanobubbles helped reducing the quantity of surfactant required to reach good foamability.

Summary of key improvements compared to literature

This study confirms the effect of bulk nanobubbles on gas-liquid mixtures and complement the findings from Ushida *et al.* (2012) and later Yesui *et al.* (2018) showing that the presence of nanobubbles in solution could affect various gas-liquid interfacial properties [22] [23].

This work validates the hypothesis that bulk nanobubbles can affect significantly Colloid systems. This important role was first stressed out by Zhang and Seddon (2016, 2019) with their study of the impact of nanobubbles on the stability of nanoparticles dispersions [24,25].

These findings corroborate the effect observed by Sobhy and Tao (2019) that found for the first time, that froth stability was improved by nanobubbles in the presence of strongly hydrophobic particles [27]. Nevertheless, up to now, few studies had been undertaken to determine if these nanobubbles could affect dispersed colloidal systems such as foams or emulsions. Therefore, this unique, systematic and controlled study brings forward the research in the field. Indeed, it demonstrates for the first time that bulk nanobubbles generated by microfluidics in a well-controlled and reproducible way, can affect significantly aqueous surfactant stabilized foams.

Summary of hypothesis, new concepts and innovations

From a practical point of view, these results suggest that processing effects can be important: a pre-foaming process (shaking, gas incorporation, etc.) that could provide the generation of NBs within the solution, could have an impact on the final foaming process. For example, a surfactant solution which is first "nanobubbled" (i.e, gas is injected to create NBs) will have different properties than the same solution without nanobubbles. Thereby, nanobubbles need to be considered when comparing chemical systems. Indeed, uncontrolled presence of nanobubbles, unintentionally included in the process, can play a non-expected role at the scale of the thin films separating bubbles and modify the gas-liquid interfacial properties. Finally, this study has proven that nanobubbles can help stabilising larger bubbles. For instance, nanobubbles could potentially be employed to reduce the concentration of stabilizers in foamed dairy products (such as ice cream), or in cosmetics, and thus reducing production costs, fat or synthetic compounds and the impact of these products on the environment.

Vision of future work

Despite the clear progress in the research brought by this study, additional investigations are required to elucidate the microscopic mechanisms linked to the presence of nanobubbles in micro-/macro-bubble foams. Further work is needed to study the effect of bulk nanobubbles concentration on surfactant-stabilized foam stability. In addition, alternative surfactant, surfactant-nanobubble solutions and resulting foam properties could be analysed to better identify the effect of bulk nanobubbles on such colloidal system.

ACKNOWLEDGEMENTS

This work was partially supported by the Engineering and Physical Sciences Research Council (grant number EP/R004382/1).

REFERENCES

[1] A. Saint-Jalmes, D. Langevin, Time evolution of aqueous foams: drainage and coarsening, J. Phys. Condens. Matter. 14 (2002) 9397. http://stacks.iop.org/0953-8984/14/i=40/a=325.

[2] A. Saint-Jalmes, Physical chemistry in foam drainage and coarsening, Soft Matter. 2 (2006) 836–849. https://doi.org/10.1039/B606780H.

[3] E.D. Manev, A. V Nguyen, Effects of surfactant adsorption and surface forces on thinning and rupture of foam liquid films, Int. J. Miner. Process. 77 (2005) 1–45. https://doi.org/https://doi.org/10.1016/j.minpro.2005.01.003.

[4] T.N. Hunter, R.J. Pugh, G. V Franks, G.J. Jameson, The role of particles in stabilising foams and emulsions, Adv. Colloid Interface Sci. 137 (2008) 57–81. https://doi.org/https://doi.org/10.1016/j.cis.2007.07.007.

[5] B.P. Binks, T.S. Horozov, Aqueous Foams Stabilized Solely by Silica Nanoparticles, Angew. Chemie Int. Ed. 44 (2005) 3722–3725. https://doi.org/10.1002/anie.200462470.

[6] R. Petkova, S. Tcholakova, N.D. Denkov, Foaming and Foam Stability for Mixed Polymer–Surfactant Solutions: Effects of Surfactant Type and Polymer Charge, Langmuir. 28 (2012) 4996–5009. https://doi.org/10.1021/la3003096.

[7] Z.A. AlYousef, M.A. Almobarky, D.S. Schechter, The effect of nanoparticle aggregation on surfactant foam stability, J. Colloid Interface Sci. 511 (2018) 365–373. https://doi.org/https://doi.org/10.1016/j.jcis.2017.09.051.

[8] F. Guo, S. Aryana, An experimental investigation of nanoparticle-stabilized CO2 foam used in enhanced oil recovery, Fuel. 186 (2016) 430–442. https://doi.org/10.1016/j.fuel.2016.08.058.

[9] N. Yekeen, M.A. Manan, A.K. Idris, E. Padmanabhan, R. Junin, A.M. Samin, A.O. Gbadamosi, I. Oguamah, A comprehensive review of experimental studies of nanoparticles-

stabilized foam for enhanced oil recovery, J. Pet. Sci. Eng. 164 (2018) 43–74. https://doi.org/https://doi.org/10.1016/j.petrol.2018.01.035.

[10] P. Nguyen, H. Fadaei, D. Sinton, Pore-Scale Assessment of Nanoparticle-Stabilized CO2 Foam for Enhanced Oil Recovery, Energy & Fuels. 28 (2014) 6221–6227. https://doi.org/10.1021/ef5011995.

[11] S. Andrieux, W. Drenckhan, C. Stubenrauch, Highly ordered biobased scaffolds: From liquid to solid foams, Polymer (Guildf). 126 (2017) 425–431. https://doi.org/10.1016/j.polymer.2017.04.031.

[12] S. Andrieux, W. Drenckhan, C. Stubenrauch, Generation of Solid Foams with Controlled Polydispersity Using Microfluidics, Langmuir. (2018). https://doi.org/10.1021/acs.langmuir.7b03602.

[13] J.R.T. Seddon, D. Lohse, W.A. Ducker, V.S.J. Craig, A Deliberation on Nanobubbles at Surfaces and in Bulk, ChemPhysChem. 13 (2012) 2179–2187. https://doi.org/10.1002/cphc.201100900.

[14] S.H. Oh, J.-M. Kim, Generation and Stability of Bulk Nanobubbles, Langmuir. (2017). https://doi.org/10.1021/acs.langmuir.7b00510.

[15] M. Alheshibri, J. Qian, M. Jehannin, V.S.J. Craig, A History of Nanobubbles, Langmuir. 32 (2016) 11086–11100. https://doi.org/10.1021/acs.langmuir.6b02489.

[16] G. Liu, Z. Wu, V.S.J. Craig, Cleaning of protein-coated surfaces using nanobubbles: An investigation using a Quartz Crystal Microbalance, J. Phys. Chem. C. 112 (2008) 16748–16753. https://doi.org/10.1021/jp805143c.

[17] H. Chen, H. Mao, L. Wu, J. Zhang, Y. Dong, Z. Wu, J. Hu, Defouling and cleaning using nanobubbles on stainless steel, Biofouling. 25 (2009) 353–357. https://doi.org/10.1080/08927010902807645.

[18] M. Fan, D. Tao, R. Honaker, Z. Luo, Nanobubble generation and its application in froth flotation (part I): nanobubble generation and its effects on properties of microbubble and millimeter scale bubble solutions, Min. Sci. Technol. 20 (2010) 1–19. https://doi.org/https://doi.org/10.1016/S1674-5264(09)60154-X.

[19] M. Fan, D. Tao, R. Honaker, Z. Luo, Nanobubble generation and its applications in froth flotation (part II): fundamental study and theoretical analysis, Min. Sci. Technol. 20 (2010) 159–177. https://doi.org/https://doi.org/10.1016/S1674-5264(09)60179-4.

[20] N. Nirmalkar, A.W. Pacek, M. Barigou, Interpreting the interfacial and colloidal stability of bulk nanobubbles, Soft Matter. 14 (2018) 9643–9656. https://doi.org/10.1039/C8SM01949E.

[21] J.H. Weijs, J.R.T. Seddon, D. Lohse, Diffusive Shielding Stabilizes Bulk Nanobubble Clusters, ChemPhysChem. 13 (2012) 2197–2204. https://doi.org/10.1002/cphc.201100807.

[22] A. Ushida, T. Hasegawa, N. Takahashi, T. Nakajima, S. Murao, T. Narumi, H. Uchiyama, Effect of mixed nanobubble and microbubble liquids on the washing rate of cloth in an alternating flow, J. Surfactants Deterg. 15 (2012) 695–702. https://doi.org/10.1007/s11743-012-1348-x.

[23] K. Yasui, T. Tuziuti, N. Izu, W. Kanematsu, Is surface tension reduced by nanobubbles (ultrafine bubbles) generated by cavitation?, Ultrason. Sonochem. (2018). https://doi.org/https://doi.org/10.1016/j.ultsonch.2018.11.020.

[24] M. Zhang, J.R.T. Seddon, Nanobubble–Nanoparticle Interactions in Bulk Solutions, Langmuir. 32 (2016) 11280–11286. https://doi.org/10.1021/acs.langmuir.6b02419.

[25] M. Zhang, J.R.T. Seddon, S.G. Lemay, Nanoparticle–nanobubble interactions: Charge inversion and re-entrant condensation of amidine latex nanoparticles driven by bulk nanobubbles, J. Colloid Interface Sci. 538 (2019) 605–610.

https://doi.org/10.1016/j.jcis.2018.11.110.

[26] D. Tao, A. Sobhy, L. Li, Nanobubble effects on hydrodynamic interactions between particles and bubbles, Powder Technol. (2019). https://doi.org/https://doi.org/10.1016/j.powtec.2019.02.024.

[27] A. Sobhy, D. Tao, Effects of Nanobubbles on Froth Stability in Flotation Column, Int. J. Coal Prep. Util. 39 (2019) 183–198. https://doi.org/10.1080/19392699.2018.1459582.

[28] S. Calgaroto, A. Azevedo, J. Rubio, Flotation of quartz particles assisted by nanobubbles, Int. J. Miner. Process. 137 (2015) 64–70. https://doi.org/https://doi.org/10.1016/j.minpro.2015.02.010.

[29] S. Nazari, S.Z. Shafaei, M. Gharabaghi, R. Ahmadi, B. Shahbazi, Effect of frother type and operational parameters on nano bubble flotation of quartz coarse particles, J. Min. Environ. 9 (2018) 539–546. https://doi.org/10.22044/jme.2017.6404.1461.

[30] D. Vigolo, S. Buzzaccaro, R. Piazza, Thermophoresis and thermoelectricity in surfactant solutions., Langmuir. 26 (2010) 7792–7801. https://doi.org/10.1021/la904588s.

[31] N.M. Kovalchuk, M. Sagisaka, K. Steponavicius, D. Vigolo, M.J.H. Simmons, Drop formation in microfluidic cross-junction: jetting to dripping to jetting transition, Microfluid. Nanofluidics. 23 (2019) 103. https://doi.org/10.1007/s10404-019-2269-z.

[32] C. Thévenot, B. Grassl, G. Bastiat, W. Binana, Aggregation number and critical micellar concentration of surfactant determined by time-dependent static light scattering (TDSLS) and conductivity, Colloids Surfaces A Physicochem. Eng. Asp. 252 (2005) 105–111. https://doi.org/https://doi.org/10.1016/j.colsurfa.2004.10.062.

[33] P. Kim, K.W. Kwon, M.C. Park, S.H. Lee, S.M. Kim, K.Y. Suh, Soft Lithography for Microfluidics: a Review, BIiochip J. 2 (2008) 1–11. internal-pdf://0720923336/soft lithography description.pdf.

[34] L. Labarre, D. Vigolo, Microfluidics approach to investigate foam hysteretic behaviour, Microfluid. Nanofluidics. 23 (2019) 129. https://doi.org/10.1007/s10404-019-2299-6.

[35] A.E. Mark, A.J. Michael, K.G. Bruce, Determining the optimal PDMS–PDMS bonding technique for microfluidic devices, J. Micromechanics Microengineering. 18 (2008) 67001. http://stacks.iop.org/0960-1317/18/i=6/a=067001.

[36] T. Cubaud, U. Ulmanella, C.-M. Ho, Two-phase flow in microchannels with surface modifications, Fluid Dyn. Res. 38 (2006) 772–786. https://doi.org/http://dx.doi.org/10.1016/j.fluiddyn.2005.12.004.

[37] W.A.C. Bauer, M. Fischlechner, C. Abell, W.T.S. Huck, Hydrophilic PDMS microchannels for high-throughput formation of oil-in-water microdroplets and water-in-oil-in-water double emulsions, Lab a Chip - Miniaturisation Chem. Biol. 10 (2010) 1814–1819. https://doi.org/10.1039/c004046k.

[38] S.A. Peyman, R.H. Abou-Saleh, J.R. McLaughlan, N. Ingram, B.R.G. Johnson, K. Critchley, S. Freear, J.A. Evans, A.F. Markham, P.L. Coletta, S.D. Evans, Expanding 3D geometry for enhanced on-chip microbubble production and single step formation of liposome modified microbubbles, Lab Chip. 12 (2012) 4544–4552. https://doi.org/10.1039/C2LC40634A.

[39] S.A. Peyman, J.R. McLaughlan, R.H. Abou-Saleh, G. Marston, B.R.G. Johnson, S. Freear, P.L. Coletta, A.F. Markham, S.D. Evans, On-chip preparation of nanoscale contrast agents towards high-resolution ultrasound imaging, Lab Chip. 16 (2016) 679–687. https://doi.org/10.1039/C5LC01394A.

[40] L.L. Schramm, Emulsions, Foams, and Suspensions: Fundamentals and Applications, Wiley-VCH Verlag GmbH & Co. KGaA, Weinheim, 2006. https://doi.org/10.1002/3527606750.

[41] E. Nowak, Z. Xie, N.M. Kovalchuk, O.K. Matar, M.J.H. Simmons, Bulk advection and interfacial flows in the binary coalescence of surfactant-laden and surfactant-free drops, Soft Matter. 13 (2017) 4616–4628. https://doi.org/10.1039/C7SM00328E.

[42] N. Nirmalkar, A.W. Pacek, M. Barigou, On the Existence and Stability of Bulk Nanobubbles, Langmuir. 34 (2018) 10964–10973. https://doi.org/10.1021/acs.langmuir.8b01163.

[43] B. Janczuk, J.M. Bruque, M.L. Gonzalez-Martin, C. Dorado-Calasanz, The Adsorption of Triton X-100 at the Air-Aqueous Solution Interface, Langmuir. 11 (1995) 4515–4518. https://doi.org/10.1021/la00011a055.

[44] J. Eastoe, J.S. Dalton, Dynamic surface tension and adsorption mechanisms of surfactants at the air–water interface, Adv. Colloid Interface Sci. 85 (2000) 103–144. https://doi.org/http://dx.doi.org/10.1016/S0001-8686(99)00017-2.